J Electr Eng Technol.2015; 10(3): 1025-1034
http://dx.doi.org/10.5370/JEET.2015.10.3.1025

ISSN(Print) 1975-0102
ISSN(Online) 2093-7423

Improved Method for Calculating Magnetic Field of Surface-Mounted Permanent Magnet Machines Accounting for Slots and Eccentric Magnet Pole

Yu Zhou†, Huaishu Li*, Wei Wang, Qing Cao* and Shi Zhou***

Abstract – This paper presented an improved analytical method for calculating the open-circuit magnetic field in the surface-mounted permanent magnet machines accounting for slots and eccentric magnet pole. Magnetic field produced by radial and parallel permanent magnet is equivalent to that produced by surface current according to equivalent surface-current method of permanent magnet. The model is divided into two types of subdomains. The field solution of each subdomain is obtained by applying the interface and boundary conditions. The magnet field produced by equivalent surface current is superposed according to superposition principle of vector potential. The investigation shows harmonic contents of radial flux density can be reduced a lot by changing eccentric distance of eccentric magnet poles compared with conventional surface-mounted permanent-magnet machines with concentric magnet poles. The FE(finite element) results confirm the validity of the analytical results with the proposed model.

Keywords: Permanent magnet machines, Magnetic field, Eccentric magnet pole, Surface current

1. Introduction

Permanent-magnet machines have become more and more popular in the commercial, industrial and military products benefiting from higher power ratio to mass, torque ratio to volume, efficiency and lower vibration and noise over conventional electrically produced synchronous machines and asynchronous machines [1-3]. The magnetic field distribution in the air-gap is one of the most important issues in the permanent-magnet machines. It is foundation to other issues. At the present time, the numerical methods for magnetic field calculation, such as finite-elements method, provide accurate results concerning all kinds of magnetic sizes of permanent magnet machines, taking into account the saturation and without making any simplification of the geometry. But the numerical methods are very time-consuming, not suit to the initial design and optimization of the machines. Usually, the numerical methods are very good for the adjustment and validation of the design. Furthermore, the results which are obtained by numerical methods may be not accurate to calculate cogging torque and unbalanced magnetic force [4, 5] since it is sensitive to the FE meshes. Indeed, the motor performance can be obtained by the analytical methods of field computation based on the sufficient hypotheses [7].

Zhu [8] worked for both internal and external rotor motor topologies, and either radial or parallel magnetized magnets by accounting for the effects of both the magnets and the stator windings. B. Ackermann [9] proposed a two-step method, solving slotless field firstly and predicting the slotting effect based on slotless field, to reduce the computational complexity for each rotor position, although slotting effect still needs to be evaluated for all rotor positions. The method is very quick but is an approximate method. P. Kumar [10] developed an analytical model for the instantaneous air-gap field density with the assumption that the iron (both stator and rotor yoke) has finite permeability and the thickness of the stator yoke is finite. The slotting effect can be accounted for by the conformal mapping method which transforms the field solution in the corresponding slotless domain into the slotted domain. One typical example is the Carter's factor which compensates the main flux for the slotting effect. F.W. Carter applied the conformal transformation to calculate magnetic field of electrically produced machines accounting for the slots [11] firstly. Cogging torque, acoustic noise and vibration spectra can not be analyzed by use of Carter's coefficient.

It is very important to take into account slots in the analytical methods. Liu [11, 12] presents an analytical model suitable for analyzing permanent magnet motors with slotted stator core which calculate the air-gap flux density taking into account the effect of the interaction between the pole transitions and slot openings and solving the governing functions. In [7], the interface of magnet field between slots and air gap was obtained in form of Fourier

† Corresponding Author: College of Electrical Engineering, Naval University of Engineering, Wuhan, China. (zhouyu_engineer@hotmail.com)
* College of Electrical Engineering, Naval University of Engineering, Wuhan, China. (249988184@qq.com)
** Power China Zhongnan Engineering Corporation limited, ChangSha, China. (352265161@qq.com)
Received: May 17, 2014; Accepted: January 5, 2015

series. Its high accuracy for the flux density distributions in both air-gap and magnets of the machines with different slot opening widths was confirmed by FE. Zhu [14] extended [7] to account for any pole and slot combinations, and an accurate analytical subdomain model with stator slotting effects was presented for computation of the open-circuit magnetic field in surface-mounted permanent magnet machines. Some mistakes were clarified at the same time. Wu [15] developed an improved analytical subdomain model for calculating the open-circuit magnetic field in surface-mounted permanent magnet machines accounting for the tooth-tips in the slots based on 2-D polar coordinate.

In [7], and [11-14], the field domain was divided into some types of subdomains, and calculated according to interface and boundary condition. The radial and circumferential components of magnet magnetization were expressed in the form of Fourier series to solve Possion equation in the concentric permanent magnet. But the interface between eccentric permanent magnet and air-gap is very difficult to be obtained. K. Boughrara [16] used two-dimensional field theory in polar coordinates to determine the flux density distribution, cogging torque, back EMF and electromagnetic torque in the slotted air gap of permanent-magnet motors with surface mounted magnet bars which are magnetized in shifting direction, but not like Halbach array magnetization. The sinusoidal waveform of the flux density distribution was obtained, but installation process of the permanent magnet bars is not easy to achieve.

Eccentric magnet pole is a typical example of eccentric magnet pole, and performance of motors can be optimized by changing eccentric distance of the eccentric magnet poles. Zhang[17] deduced expressions of Fourier transform coefficient for magnetomotive force of eccentric magnet pole. The main exciting force wave can be reduced through suitable selection of the eccentric distance. Xu [18] analyzed the influence of the eccentric magnet poles on the waveform of air-gap flux density and the motor performances, proposed a novel optimal designing method for the eccentric magnet poles with analytical expression. In [19], based on the magnetic field which was produced by a pair of windings on the air-gap, the expressions of the flux density produced by parallel-magnetized permanent magnet with different shapes were deduced with surface-current method. But slots were not accounted. At the present time, the analytical model of permanent-magnet machines accounting for eccentric magnet poles and slots has not been analyzed comprehensively.

In this paper, an improved analytical method accounting for slots and eccentric magnet pole is derived for calculating the magnetic field distribution of machine. In the derivation, magnetic field produced by radial and parallel eccentric permanent magnet is equivalent to that produced by surface current according to surface-current method of permanent magnet. The field domain is divided into two types of subdomains. The analytical field expressions of two subdomains produced by a pair of windings are obtained by the variable separation method. The coefficients in the field expressions are determined by applying the interface and boundary conditions. The magnet field produced by equivalent surface current is superposed according to superposition principle of vector potential. Compared with conventional surface-mounted permanent-magnet machines with concentric magnet poles, harmonic content of radial flux density can be reduced a lot by changing eccentric distance of eccentric magnet poles. The investigation shows the developed model has high accuracy to calculate the flux density of surface-mounted permanent magnet machines with eccentric magnet poles. The finite element (FE) results verify the validity of the analytical model.

2. Analytical Field Modeling

2.1 Equivalent surface current of magnet pole

In this paper, the analytical modeling is based on the following assumptions:

(1) Linear properties of permanent magnet;
(2) Infinite permeable iron materials;
(3) The relative permeability in the PM is equal to1;
(4) Negligible end effect;
(5) Simplified slot as shown in Fig. 1.

The two-dimensional conventional subdomain model is shown in Fig. 1. The magnet field is divided into two types of subdomains for the convenience of analysis: (1) subdomain of permanent magnet and air-gap (The first subdomain is limited by a circle characterised by a R_s radius); (2) subdomain of slots.

The permanent magnet with eccentric structure is shown

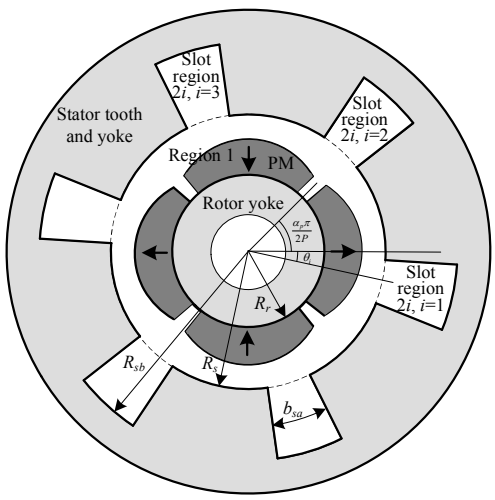

Fig. 1. Symbols and types of subdomains.

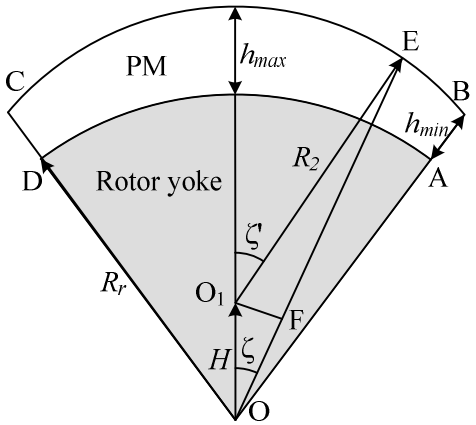

Fig. 2. The eccentric structure of permanent magnet

in Fig. 2. The distance between point E and point O can be given by

$$OE = H * \cos\zeta + \sqrt{(R_r + h_{\max} - H)^2 - (H * \sin\zeta)^2} \quad (1)$$

where H is the eccentric distance, R_r is the radius of rotor, h_{max} is the maximum thickness of permanent magnet and ζ is the radian between OE and the center line of permanent magnet.

The radian between O_1E and the center line of permanent magnet can be given by

$$\zeta' = arc\sin(OE * \sin\zeta / R_2) \quad (2)$$

where R_2 is the radius of arc BC.

The radius of arc BC can be given by

$$R_2 = R_r + h_{\max} - H \quad (3)$$

The eccentric distance of the permanent magnet can be given by

$$H = \frac{(h_{\max} - h_{\min})(2R_r + h_{\max} + h_{\min})}{2(R_r + h_{\max}) - 2(R_r + h_{\min})\cos[\alpha_p \pi / (2P)]} \quad (4)$$

where $h_{\min}$ is the minimum thickness of PM, α_p is pole-arc to pole-pitch ratio and P is pole pairs.

The equivalent surface current is equal to the circumferential component of coercivity on the surface of magnet pole[19]. And the equivalent surface current of eccentric magnet pole is shown in Fig. 3(a) for parallel magnetization.

The current density of AB and CD can be given by

$$J_1 = H_{cj}\cos[\alpha_p \pi / (2P)] \quad (5)$$

where H_{cj} is coercivity of permanent magnet.

The surface current density of side BC can be given by

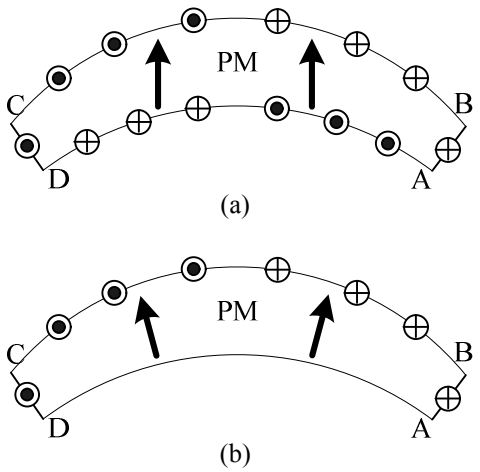

Fig. 3. Equivalent surface current of eccentric magnet pole. (a) Parallel magnetization; (b) Radial magnetization.

$$J_2 = H_{cj}\sin\zeta' \quad (6)$$

The surface current density of side AD can be given by

$$J_3 = H_{cj}\sin\zeta \quad (7)$$

The equivalent surface current of eccentric magnet pole is shown in Fig. 3(b) for radial magnetization.

The surface current density of side AB and CD can be given by

$$J_1 = H_{cj} \quad (8)$$

The surface current density of side BC can be given by

$$J_2 = H_{cj}\sin(\zeta' - \zeta) \quad (9)$$

The surface current density of side AD is zero.

2.2 Magnet field produced by a pair of windings

Equivalent surface-current method is based on magnet field produced by a pair of windings. The current of windings can be given by

$$i_c = J_x \Delta l \quad (x = 1,\ 2,\ 3)$$

where Δl is the length infinitesimal in the side AB, CD, AD and BC of magnet pole.

In this section, magnet field produced by a pair of windings is analyzed. Subdomain model with a pair of windings is shown in Fig. 4.

2.2.1 Magnet field in the first type of subdomains

Since in the 2-D field, the vector potential has only z-axis component which satisfies:

$$\frac{\partial A_{z1}{}^2}{\partial r^2}+\frac{1}{r}\frac{\partial A_{z1}}{\partial r}+\frac{1}{r^2}\frac{\partial A_{z1}{}^2}{\partial \theta^2}=0 \tag{10}$$

α and β are the labels of winding. a and ζ present the position of the windings in the polar coordinate system. i_c is current. The vector potential of point $Q(r,\theta)$ produced by α and β is given by

$$A_{Z1}^{\alpha}=-\frac{\mu_0 i_c}{2\pi}\ln\rho_\alpha+\sum_m[(A_{m1}^{\alpha}r^m+B_{m1}^{\alpha}r^{-m})\cos(m(\theta-\zeta))]+\sum_m[(C_{m1}^{\alpha}r^m+D_{m1}^{\alpha}r^{-m})\sin(m(\theta-\zeta))] \tag{11}$$

and

$$A_{Z1}^{\beta}=\frac{\mu_0 i_c}{2\pi}\ln\rho_\beta+\sum_m[(A_{m1}^{\beta}r^m+B_{m1}^{\beta}r^{-m})\cos(m(\theta+\zeta))]+\sum_m[(C_{m1}^{\beta}r^m+D_{m1}^{\beta}r^{-m})\sin(m(\theta+\zeta))] \tag{12}$$

respectively.

According to (11) and (12), the sum of vector potential can be given by

$$A_{Z1}=-\frac{\mu_0 i_c}{2\pi}\ln\rho+\sum_m[(A_{m1}r^m+B_{m1}r^{-m})\cos(m\theta)]+\sum_m[(C_{m1}r^m+D_{m1}r^{-m})\sin(m\theta)] \tag{13}$$

where A_{m1}, B_{m1}, C_{m1}, D_{m1} are coefficients to be determined, μ_0 is the permeability of the air, r is the radial of point Q, θ is the degree between point Q and center line of the windings, ρ_α and ρ_β are the coordinates when the origins are α and β respectively.

If the origin is point O, $\ln\rho_\alpha$ and $\ln\rho_\beta$ can be expanded into infinite series about θ and r.

$$\ln\rho=\ln\rho_\alpha-\ln\rho_\beta=\begin{cases}-2\sum_m\frac{1}{m}(\frac{a}{r})^m\sin(m\zeta)\sin(m\theta), & r>a\\ -2\sum_m\frac{1}{m}\sin(m\zeta)\sin(m\theta), & r=a\\ -2\sum_m\frac{1}{m}(\frac{r}{a})^m\sin(m\zeta)\sin(m\theta), & r<a\end{cases} \tag{14}$$

The radial and circumferential components of flux density can be obtained from the vector potential distribution by

$$B_\theta=-\frac{\partial A_z}{\partial r}\quad\text{and}\quad B_r=\frac{1}{r}\frac{\partial A_z}{\partial\theta} \tag{15}$$

While $r<a$, the flux density in the first subdomain can be given by

$$B_{\theta1}=-\sum_m\left(mA_{m1}r^{m-1}-mB_{m1}r^{-m-1}\right)\cos(m\theta)-\sum_m\left[mC_{m1}r^{m-1}-mD_{m1}r^{-m-1}+\frac{\mu_0 i_c}{2\pi}\left(\frac{r}{a}\right)^{m-1}\sin(m\zeta)\right]\sin(m\theta) \tag{16}$$

for the circumferential component.

In the outer surface of rotor, the circumferential component of the flux density is zero

$$B_{\theta1}\big|_{r=R_r}=0 \tag{17}$$

Substituting (16) into (17), B_{m1} and D_{m1} can be given by

$$B_{m1}=A_{m1}R_r{}^{2m} \tag{18}$$

$$D_{m1}=\frac{\mu_0 i_c}{m\pi}\frac{R_r{}^{2m}}{a^m}\sin(m\zeta)+C_{m1}R_r{}^{2m} \tag{19}$$

While $r>a$, substituting (18) and (19) into (13), the general solution of vector field in the first subdomain can be given by

$$A_{Z1}=\sum_m A_{m1}G_{1m}\cos(m\theta)+\sum_m\left(C_{m1}G_{1m}+G_{0m}r^{-m}\right)\sin(m\theta) \tag{20}$$

where

$$G_{1m}=r^m+R_r{}^{2m}r^{-m} \tag{21}$$

$$G_{0m}=\frac{\mu_0 i_c}{m\pi}\frac{R_r{}^{2m}+a^{2m}}{a^m}\sin(m\zeta) \tag{22}$$

While $r>a$, the flux density in the first subdomain can be given by

$$B_{r1}=\frac{m}{r}[-\sum_m A_{m1}G_{1m}\sin(m\theta)+\sum_m\left(C_{m1}G_{1m}-G_{0m}r^{-m}\right)\cos(m\theta)] \tag{23}$$

for the radial component, and

$$B_{\theta1}=-\frac{1}{r}[\sum_m A_{m1}G_{2m}\cos(m\theta)+\sum_m\left(C_{m1}G_{2m}-G_{3m}\right)\sin(m\theta)] \tag{24}$$

for the circumferential component, where

$$G_{2m} = m(r^m - {R_r}^{2m} r^{-m}) \tag{25}$$

$$G_{3m} = \frac{\mu_0 i}{\pi} \frac{{R_r}^{2m} + a^{2m}}{a^m} r^{-m} \sin(m\zeta) \tag{26}$$

The vector potential produced by the equivalent surface current of *j*th magnet pole can be given by:

$$A_{Z1j} = \sum_m A_{mj} G_{1m} \cos\{m[\theta + (j-1)\pi / P]\} + \sum_m (C_{mj} G_{1m} + G_{0mj} r^{-m}) \sin\{m[\theta + (j-1)\pi / P]\} \tag{27}$$

$$G_{0mj} = (-1)^{j-1} \frac{\mu_0 i_c}{m\pi} \frac{{R_r}^{2m} + a^{2m}}{a^m} \sin(m\zeta) \tag{28}$$

where A_{mj} and C_{mj} are coefficients to be determined, and $(j-1)\pi / P$ is the angle between center line of first pole and that of *j*th pole.

2.2.2 Magnet field in the second type of subdomains

The governing function in the slots is:

$$\frac{\partial {A_{z2i}}^2}{\partial r^2} + \frac{1}{r}\frac{\partial A_{z2i}}{\partial r} + \frac{1}{r^2}\frac{\partial {A_{z2i}}^2}{\partial \theta^2} = 0 \tag{29}$$

The vector potential in the subdomain *2i* is[15]

$$A_{z2i} = \sum_n D_{n2i} \left[G_{4n} \left(\frac{r}{R_{sb}} \right)^{E_n} + \left(\frac{r}{R_s} \right)^{-E_n} \right] * \cos\left[E_n \left(\theta + b_{sa}/2 - \theta_i \right) \right] \tag{30}$$

where R_s is the inner radial of the stator, R_{sb} is the radial of the slot bottom, θ_i is the angle between center line of the *i*th slot and center line of the windings as shown in Fig. 4, b_{sa} is the slot opening width angle, D_{n2i} is coefficient to be determined, and

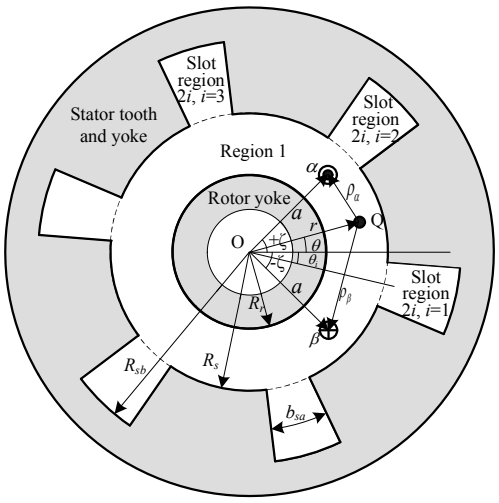

Fig. 4. Subdomain model with a pair of windings

$$E_n = n\pi / b_{sa} \tag{31}$$

$$G_{4n} = (R_s / R_{sb})^{En} \tag{32}$$

So the flux density in the second subdomain can be given by

$$B_{r2i} = -\sum_n E_n D_{n2i} \left[\frac{G_{4n}}{R_{sb}} \left(\frac{r}{R_{sb}} \right)^{E_n - 1} + \frac{1}{R_s} \left(\frac{r}{R_s} \right)^{-E_n - 1} \right] * \sin\left[E_n \left(\theta + b_{sa}/2 - \theta_i \right) \right] \tag{33}$$

for the radial component, and

$$B_{\theta 2i} = -\sum_n E_n D_{n2i} \left[\frac{G_{4n}}{R_{sb}} \left(\frac{r}{R_{sb}} \right)^{E_n - 1} - \frac{1}{R_s} \left(\frac{r}{R_s} \right)^{-E_n - 1} \right] * \cos\left[E_n \left(\theta + b_{sa}/2 - \theta_i \right) \right] \tag{34}$$

for the circumferential component.

2.2.3 Interface condition between two types of subdomain

(a) The First Interface Condition

The first interface condition is that the circumferential component of the flux density in the inner surface of stator $r=R_s$ is equal.

By evaluating (34) at the $r=R_s$ interface, (34) simplifies down to

$$B_{\theta 2i}\big|_{r=R_s} = \sum_n B_{i\theta n} \cos\left[E_n \left(\theta + b_{sa}/2 - \theta_i \right) \right] \tag{35}$$

where

$$B_{i\theta n} = -E_n D_{n2i} ({G_{4n}}^2 - 1) / R_s \tag{36}$$

The circumferential component of the flux density along the stator bore outside the slot is zero since the stator core material is infinitely permeable. So Fourier series of the circumferential component of the flux density in the inner surface of stator can be given by

$$B_{s\theta 2} = \sum_m \left[C_{ms} \cos(m\theta) + D_{ms} \sin(m\theta) \right] \tag{37}$$

Where

$$\begin{aligned} C_{ms} &= \frac{1}{\pi} \int_0^{2\pi} B_{s\theta 2} \cos(m\theta) d\theta \\ &= \frac{1}{\pi} \sum_i \sum_n \int_{\theta_i - b_{sa}/2}^{\theta_i + b_{sa}/2} B_{i\theta n} \cos\left[E_n (\theta + b_{sa}/2 - \theta_i) \right] * \cos(m\theta) d\theta \\ &= \sum_i \sum_n B_{i\theta n} \eta_i(n,m) \end{aligned} \tag{38}$$

$$D_{ms} = \frac{1}{\pi}\int_0^{2\pi} B_{s\theta 2}\sin(m\theta)d\theta = \frac{1}{\pi}\sum_i\sum_n\int_{\theta_i-b_{sa}/2}^{\theta_i+b_{sa}/2} B_{i\theta n}\cos\left[E_n(\theta+b_{sa}/2-\theta_i)\right] * \sin(m\theta)d\theta = \sum_i\sum_n B_{i\theta n}\xi_i(n,m) \quad (39)$$

Where

$$\eta_i(n,m) = -\frac{1}{\pi}\frac{m}{E_n{}^2-m^2}[\cos(n\pi)\sin(m\theta_i+mb_{sa}/2) - \sin(m\theta_i-mb_{sa}/2)] \quad (40)$$

$$\xi_i(n,m) = \frac{1}{\pi}\frac{m}{E_n{}^2-m^2}[\cos(n\pi)\cos(m\theta_i+mb_{sa}/2) - \cos(m\theta_i-mb_{sa}/2)] \quad (41)$$

According to the vector potential distribution in the first subdomain, the circumferential component of the flux density in the inner surface of stator can be given as

$$B_{s\theta 2} = B_{\theta 1}\big|_{r=R_s} \quad (42)$$

According to (24), (37) and (42):

$$\begin{cases} G_{2m}^{r=R_s}A_{m1} = -R_sC_{ms} \\ G_{2m}^{r=R_s}C_{m1} - G_{3m}^{r=R_s} = -R_sC_{ms} \end{cases} \quad (43)$$

Combining (36), (38), (39) and (43), the following equations can be obtained:

$$\begin{cases} \mathrm{K_{11}A_1+K_{13}D_{2i}=0} \\ \mathrm{K_{22}C_1+K_{23}D_{2i}=Y_2} \end{cases} \quad (44)$$

(b) The Second Interface Condition

The second interface condition is that the vector potential of the *i*th slot opening is equal in the two types of the subdomains.

According to (20), the vector potential in the inner surface of stator can be given as

$$A_s = A_{Z1}\big|_{r=R_s} = \sum_m\left[A_{mc}\cos(m\theta)+A_{ms}\sin(m\theta)\right] \quad (45)$$

where

$$A_{mc} = G_{1m}^{r=R_s}A_m \quad (46)$$

$$A_{ms} = G_{1m}^{r=R_s}C_m + G_{0m}R_s^{-m} \quad (47)$$

The equation (45) can be expanded into Fourier series along the stator inner surface of the ith slot:

$$A_s = \sum_n A_{ni}\cos[E_n(\theta+b_{sa}/2-\theta_i)], \quad (\theta_i-b_{sa}/2\le\theta\le\theta_i+b_{sa}/2) \quad (48)$$

$$A_{ni} = \frac{2}{b_{sa}}\int_{\theta_i-b_{sa}/2}^{\theta_i+b_{sa}/2}\sum_{\mathrm{m}}[A_{mc}\cos(m\theta)+A_{ms}\sin(m\theta)] * \cos[E_n(\theta+b_{sa}-\theta_i)]d\theta = \sum_m(A_{mc}\sigma_i(n,m)+A_{ms}\tau_i(n,m)) \quad (49)$$

Where

$$\sigma_i(n,m) = \frac{2\pi}{b_{sa}}\eta_i(n,m) \quad (50)$$

$$\tau_i(n,m) = \frac{2\pi}{b_{sa}}\xi_i(n,m) \quad (51)$$

According to (30), the vector potential in the inner surface of stator can be obtained:

$$A_{z2i}\big|_{r=R_s} = \sum_n D_{n2i}(G_{4n}^2+1)\cos[E_n(\theta+b_{sa}-\theta_i)] \quad (52)$$

The vector potential in the inner surface of stator is equal in two subdomains.

$$A_{z2i}\big|_{r=R_s} = A_s \quad (53)$$

Substituting (48) and (52) into (53), the following equation can be obtained:

$$\sum_n D_{n2i}(G_{4n}^2+1)\cos[E_n(\theta+b_{sa}-\theta_i)] = \sum_n A_{ni}\cos[E_n(\theta+b_{sa}/2-\theta_i)] \quad (54)$$

Then

$$D_{n2i}(G_{4n}^2+1) = A_{ni} \quad (55)$$

Substituting (49) into (55), the following equation can be obtained:

$$D_{n2i}(G_{4n}^2+1) = \sum_m(A_{mc}\sigma_i(n,m)+A_{ms}\tau_i(n,m)) \quad (56)$$

while n=1, 2, 3….

Combining (46), (47) and (53), the following equation can be obtained:

$$\mathrm{K_{31}A_1+K_{32}C_1+K_{33}D_{2\,i}=Y_3} \quad (57)$$

According to (44) and (57), the matrix format can be

given as

$$\begin{bmatrix} K_{11} & 0 & K_{13} \\ 0 & K_{22} & K_{23} \\ K_{31} & K_{32} & K_{33} \end{bmatrix} \begin{bmatrix} A_1 \\ C_1 \\ D_{2i} \end{bmatrix} = \begin{bmatrix} 0 \\ Y_2 \\ Y_3 \end{bmatrix} \tag{58}$$

Then the coefficients A1, C1 and D2i can be obtained according to (58).

2.2.4 The superposition principle of vector potential

The superposition principle can be applied to the vector potential by equivalent surface current in the surface-mounted permanent magnet machines.

In the Fig. 3, the vector potential produced by equivalent surface current of side AB and CD can be superposed:

$$A_{z11} = \sum_{k_1} A_{z1}\big|_{i_c = J_1 \Delta r}^{r = R_r + k_1 \Delta r} \tag{59}$$

where Δr is the length infinitesimal in the side AB and CD of PM and

$$k_1 = \{1, 2, \cdots, h_{\max} / \Delta r\} \tag{60}$$

The vector potential produced by equivalent surface current of side BC can be superposed:

$$A_{z12} = \sum_{k_2} A_{z1}\big|_{i_c = J_2 R_2 \Delta \gamma_1}^{r = OE} \tag{61}$$

where $\Delta \gamma_1$ is the angle infinitesimal in the side BC of PM, and the origin is point O_1,

$$k_2 = \{1, 2, \cdots, \zeta'_{\max} / \Delta \gamma_1\} \tag{62}$$

$$\zeta'_{\max} = \arcsin\{OB * \sin[\alpha_p \pi / (2P)] / R_2\} \tag{63}$$

The vector potential produced by equivalent surface current of side AD can be superposed:

$$A_{z13} = \sum_{k_3} A_{z1}\big|_{i_c = J_3 R_r \Delta \gamma_2}^{r = R_r} \tag{64}$$

where $\Delta \gamma_2$ is the angle infinitesimal in the side AD of PM, and the origin is point O,

$$k_3 = \{1, 2, \cdots, [\alpha_p \pi / (2P)] / \Delta \gamma_2\} \tag{65}$$

According to (15), (59), (61) and (64), the radial and circumferential components can be obtained.

3. Finite-Element Validation

The major parameters of two 30-pole/36-slot prototype machines which are used for validation are shown in Table 1. The minimum thickness of permanent magnet is 7mm in the prototype machine with eccentric magnet poles. And it is 12mm in the prototype machine with concentric magnet poles. The analytical prediction is compared with the linear FE prediction.

Table 1. Parameters of Prototype Machines (Unit: mm)

Stator outer diameter	520	Rotor diameter	370
Stator inner diameter	400	Slot opening	8
Magnet thickness (max)	12	Active length	460
Magnet thickness (min)	7 or 12	Stator yoke height	15
2P/Ns	30/36	Rated speed(rpm)	200
Magnetization	parallel	H_{cj} (KA/m)	980
Pole-arc to pole-pitch ratio		0.89	

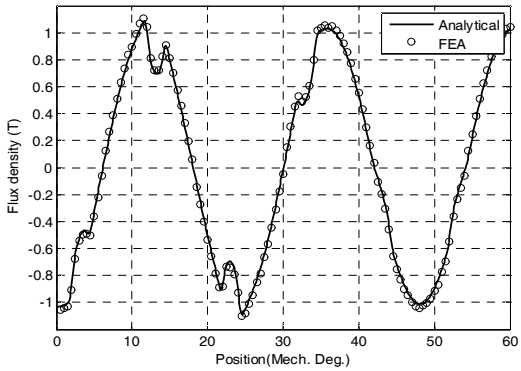

(a)

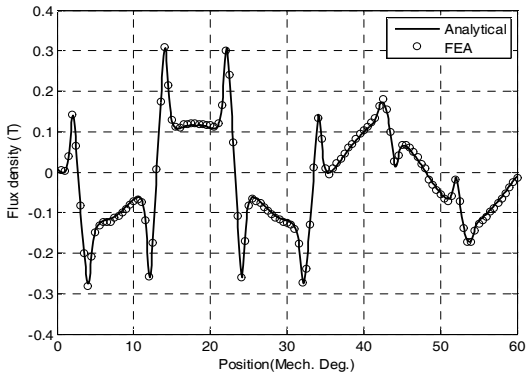

(b)

Fig. 5. FE and analytically predicted flux density waveforms in the air-gap at r=198.5mm of motor with eccentric magnet poles: (a) Radial component; (b) circumferential component.

Fig. 5 show the results between analytical and FE predictions of flux density in the air-gap at r=198.5mm of motor with eccentric magnet poles. Fig. 6 show the results between analytical and FE predictions of flux density in the air-gap at r=198.5mm of motor with concentric magnet poles. As can be seen, the predicted flux density by subdomain model with equivalent surface-current method

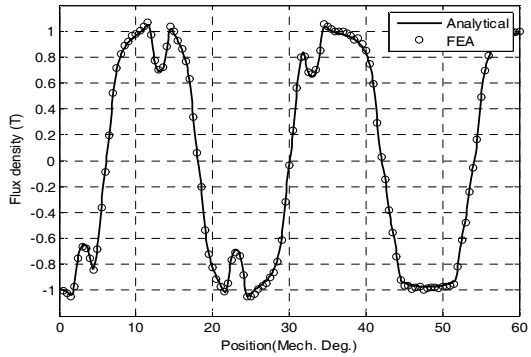

(a)

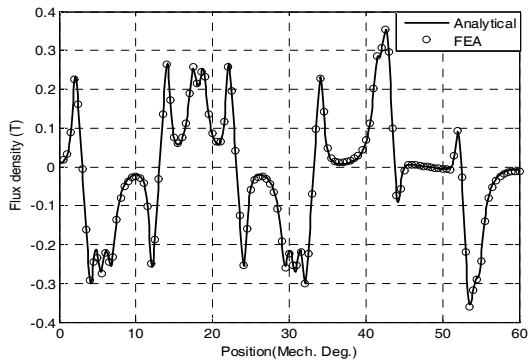

(b)

Fig. 6. FE and analytically predicted flux density waveforms in the air-gap at $r = 198.5$mm of motor with concentric magnet poles: (a) Radial component; (b) circumferential component.

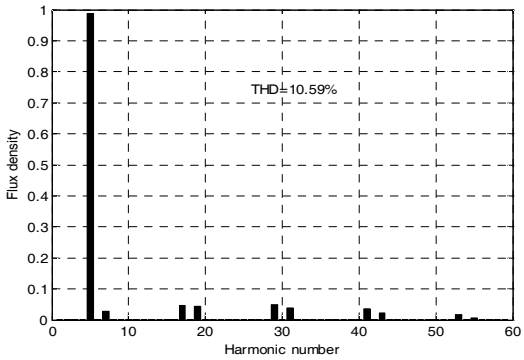

(a)

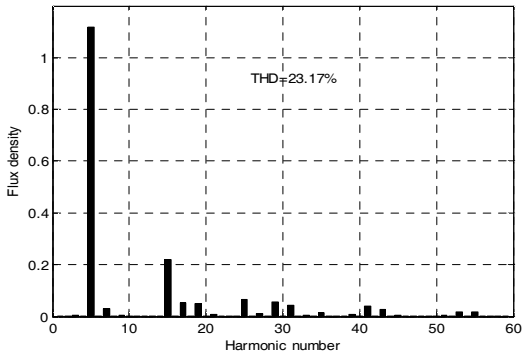

(b)

Fig. 7. Harmonic analysis of radial component of flux density at $r = 198.5$mm of motor. (a) Eccentric magnet poles; (b) Concentric magnet poles.

almost completely matches FE results.

Harmonic analysis of radial component of flux density with five pair of magnet poles in air-gap is shown in Fig. 7. Because five pair of magnet poles are one cycle to radial component of flux density in the air-gap. Then the 5th order spatial harmonic is fundamental harmonic. The same harmonic orders are 7th, 17th, 19th, 29th 31th et al. because of the influence of slots. The main different harmonic orders between Eccentric magnet poles and concentric magnet poles are the 15th and 25th order spatial harmonic. The harmonic content of radial component of flux density is 10.59% in the motor with eccentric magnet poles. The harmonic content of radial component of flux density is 23.17% in the motor with concentric magnet poles.

4. Conclusion

This paper presented an improved method for calculating the magnetic field in the surface-mounted permanent magnet machines accounting for slots and eccentric magnet pole. Magnetic field produced by radial and parallel eccentric permanent magnet is equivalent to that produced by surface current according to surface-current method of permanent magnet. The model is divided into two types of subdomains. The field solution of each subdomain is obtained by applying the interface and boundary conditions. The magnet field produced by equivalent surface current is superposed according to superposition principle of vector potential. The investigation shows harmonic contents of radial flux density can be reduced a lot by changing eccentric distance of eccentric magnet poles compared with conventional surface-mounted permanent-magnet machines with concentric magnet poles. The FE results confirm the validity of the analytical results with the proposed model.

References

[1] Z. Q. Zhu and D. Howe, "Electrical machines and drives for electric, hybrid, and fuel cell vehicles." *Proc. IEEE*, vol. 95, no. 4, pp. 746-765, Apr. 2007.

[2] Z. Q. Zhu and C. C. Chan, "Electrical machine topologies and tech-nologies for electric, hybrid, and fuel cell vehicles," in IEEE Vehicle Power and Propulsion Conf., 2008, pp. 1-6.

[3] A. M. El-Refaie, "Fractional-slot concentrated-windings synchronous permanent magnet machines: Opportunities and challenges," *IEEE Trans. Ind.*

Electron., vol. 57, no. 1, pp. 107-121, 2010.
[4] Y. Zhou, H. Li, G. Meng, S. Zhou, and Q. Cao. "Analytical Calculation of Magnetic Field and Cogging Torque in Surface-Mounted Permanent Magnet Machines Accounting for Any Eccentric Rotor Shape," *IEEE Trans. Ind. Electron*., published online, DOI: 10.1109/TIE.2014.2369458.
[5] D. Lin, S. L. Ho, and W. N. Fu, "Analytical Prediction of Cogging Torque in Surface-Mounted Permanent-Magnet Motors," *IEEE Trans. Magn.*, vol. 45, no. 9, pp. 3296-3302, Sep. 2009.
[6] D. H. Wang, X. H. Wang, D. W. Qiao, Y. Pei, and S. Y. Jung, "Reducing Cogging Torque in Surface-Mounted Permanent-Magnet Motors by Nonuniformly Distributed Teeth Method," *IEEE Trans. Magn.*, vol. 47, no. 9, pp. 2231-2239, Sep. 2011.
[7] F. Dubas and C. Espanet, "Analytical solution of the magnetic field in permanent-magnet motors taking into account slotting effect: No-load vector potential and flux density calculation," *IEEE Trans. Magn.*, vol. 45, no. 5, pp. 2097-2109, May 2009.
[8] Z. Q. Zhu, D. Howe, and C. C. Chan, "Improved analytical model for predicting the magnetic field distribution in brushless permanent-magnet machines," *IEEE Trans. Magn.*, vol. 38, no. 1, pp. 229-238, Jan. 2002.
[9] B. Ackermann and R. Sottek, "Analytical modeling of the cogging torque in permanent magnet motors," *Elect. Eng.*, vol. 78, no. 2, pp. 117-125, 1995.
[10] P. Kumar and P. Bauer, "Improved analytical model of a permanent-magnet brushless DC motor," *IEEE Trans. Magn.*, vol. 44, no. 10, pp. 2299-2309, Oct. 2008.
[11] B. Heller and V. Hamata, *Harmonic Field Effects in Induction Machines*. New York: Elsevier Scientific, 1977.
[12] Z. J. Liu, and J. T. Li, "Accurate prediction of magnetic field and magnetic forces in permanent magnet motors using an analytical solution," *IEEE Trans. Energy Convers*., vol. 23, no. 3, pp. 717-726, Sep. 2008.
[13] Z. J. Liu, and J. T. Li, "Analytical Solution of Air-Gap Field in Permanent-Magnet Motors Taking Into Account the Effect of Pole Transition Over Slots," *IEEE Trans. Magn.*, vol. 43, no. 10, pp. 3872-3883, Oct. 2007.
[14] Z. Q. Zhu, L. J. Wu, and Z. P. Xia, "An accurate subdomain model for magnetic field computation in slotted surface-mounted permanent-magnet machines," *IEEE Trans. Magn.*, vol. 46, no. 4, pp. 1100-1115, Apr. 2010.
[15] L. J. Wu, Z. Q. Zhu, D. Staton, M. Popescu, and D. Hawkins, "An improved subdomain model for predicting magnetic field of surface-mounted permanent magnet machines accounting for tooth-tips," *IEEE Trans. Magn.*, vol. 47, no. 6, pp. 1693-1704, Jun. 2011.
[16] K. Boughrara, B. L. Chikouche, R. Ibtiouen, D. Zarko, and O. Touhami, "Analytical model of slotted air-gap surface mounted permanent-magnet syn-chronous motor with magnet bars magnetized in the shifting direction," *IEEE Trans. Magn.*, vol. 45, no. 2, pp. 747-758, Feb. 2009.
[17] R. Zhang, X. H. Wang, and D. W. Qiao, "Reduction of exciting force wave for permanent magnet motors by eccentric magnet pole," *Proceedings of the CSEE*, vol. 30, no. 27, pp. 20-25, Sep. 2010.
[18] Y. Y. Xu, H. J. Ge, and Y. Jing. "Optimal design of eccentric magnet pole for permanent-magnet synchronous motors," *Journal of Harbin Engineering University*, vol. 34, no. 7, pp. 873-877, Jul. 2013.
[19] Y. Zhou, H. S. Li, and K. F. Huang, "Analytical calculation of air-gap magnetic field of the trapezoidal surface permanent magnet," in *Proc. IEEE CSAE*, Guangzhou, China, Nov., 2013, pp. 450-454.

Yu Zhou He received the B.S. degree and the M.S. degree in electrical engineering from the College of Electrical Engineering, Naval University of Engineering, Wuhan, China in 2005 and 2009 respectively. From 2012, he is working toward the Ph.D. degree in the College of Electrical Engineering, Naval University of Engineering, Wuhan, China. He is one of IEEE Members now. His major research interests include power electronics, and design and control of permanent-magnet machines.

Huaishu Li He received the B.S. degree and the M.S. degree in electrical engineering from the College of Electrical Engineering, Naval University of Engineering, Wuhan, China in 1986 and 1991 respectively, and the Ph.D. degree from Huazhong University of Science&Technology, Wuhan, China in 2001. From 1991, he lectures in the College of Electrical Engineering, Navy University of Engineering, Wuhan, China. His major research interests include power electronics, and design and control of permanent-magnet machines.

Wei Wang She received the B.S. degree in harbor, waterway and coastal engineering, from the School of Hydraulic Engineering, Changsha University of Science and Technology, China in 2009 and the M.S. degree in the school of Water Resources and Hydropower Engineering, Wuhan University, China in 2015. Currently, she is working in Power China Zhongnan Engineering Corporation limited.

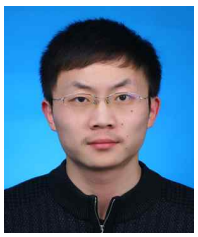

Shi Zhou He received the B.S. degree in physics from Nanjing University, Nanjing, China, in 2011. From 2013, he is working toward the M.S. degree in the College of Electrical Engineering, Naval University of Engineering, Wuhan, China. His research interest is multi-phase permanent-magnetic synchronous generator.

Qing Cao She received the B.S. degree in electric engineering from Hunan Institute of Engineering, Xiangtan, china, in 2013.She is working toward the M.S. in the College of Electrical Engineering, Naval University of Engineering, Wuhan, China. Her research interest is line-start permanent-magnetic synchronous motor.